Coherent X-ray Diffraction Imaging

Jianwei Miao, Richard L. Sandberg, and Changyong Song

(Invited Paper)

***Abstract*—For centuries, lens-based microscopy, such as optical, phase-contrast, fluorescence, confocal, and electron microscopy, has played an important role in the evolution of modern science and technology. In 1999, a novel form of microscopy, i.e., coherent diffraction imaging (also termed coherent diffraction microscopy or lensless imaging), was developed and transformed our conventional view of microscopy, in which the diffraction pattern of a noncrystalline specimen or a nanocrystal was first measured and then directly phased to obtain a high-resolution image. The well-known phase problem was solved by combining the oversampling method with iterative algorithms. In this paper, we will briefly discuss the principle of coherent diffraction imaging, present various implementation schemes of this imaging modality, and illustrate its broad applications in materials science, nanoscience, and biology. As coherent X-ray sources such as high harmonic generation and X-ray free-electron lasers are presently under rapid development worldwide, coherent diffraction imaging can potentially be applied to perform high-resolution imaging of materials/nanoscience and biological specimens at the femtosecond time scale.**

***Index Terms*—Ankylography, coherent diffraction imaging (CDI), equally sloped tomography (EST), high harmonic generation (HHG), lensless imaging, oversampling, phase retrieval, X-ray free-electron lasers (XFEL).**

I. Introduction

MICROSCOPY has found broad application in both physical and life sciences. By using novel imaging technologies and labeling techniques, optical microscopy can routinely study dynamic processes in living cells [1]. The resolution of optical microscopy ($\sim$200 nm) is limited by the wavelength of the photons in the visible region of the spectrum, although better resolutions (of up to 20 nm) may be obtained in some special cases by using super-resolution optical microscopy [2], [3]. To achieve considerably higher resolution, both shorter wavelength illumination and higher resolution lenses are required. Using magnetic lenses, transmission electron microscopy can achieve atomic resolution, but the sample has to be thinner than 50 nm [4]. For the study of surface structures, scanning probe microscopy is the predominate method and can routinely achieve atomic scale resolution [5]. To probe the structures below the surface of thick samples, X-ray imaging is the method of choice because X-rays have a longer penetration depth than electrons. However, X-rays are more difficult to focus than electrons. The highest image resolution currently achievable by X-ray optics is around 10–15 nm [6], [7].

One way to overcome this resolution barrier is to use coherent diffraction imaging (CDI) in which the diffraction pattern of a noncrystalline specimen or a nanocrystal is first measured and then directly inverted to obtain a high-resolution image [8]. The well-known phase problem is solved by combining the oversampling method [9] with iterative phase-retrieval algorithms [10]–[16]. While the idea of CDI was suggested by Sayre [17], it was not until in 1999 that the first experimental demonstration was conducted by Miao *et al.* [8]. CDI has since been applied to imaging a wide range of materials science and biological samples such as nanoparticles, nanocrystals, biomaterials, cells, cellular organelles, and viruses by using synchrotron radiation [18]–[44], high harmonic generation (HHG) and soft X-ray laser sources [45]–[49], free-electron lasers [50]–[53], and electrons [54]–[59]. An increasing number of groups have been working in this field, and several review articles have been published [60]–[67]. In this paper, we will mainly focus on the CDI methodology and its applications with X-rays. For those who are interested in coherent electron diffraction imaging as well as synchrotron X-ray holography, refer to the publications elsewhere [54]–[59], [68], [69].

II. Solution to the Noncrystallographic Phase Problem

In 1952, Sayre suggested in a short paper that by measuring the intensity of a diffraction pattern between the Bragg peaks, the lost phase information of the scattered wave might be recovered [70]. This idea was based on the fact that the autocorrelation function of an object is exactly twice the size of the object. In 1978, following Gerchberg and Saxton's work [71], Fienup developed two iterative algorithms for retrieving phases from the Fourier modulus [10], [11]. However, it was not clear at that time why the phases can be retrieved from the Fourier modulus. Subsequently, Bruck and Sodin [72], Hayes [73], and Bates [74] concluded that when the diffraction pattern of a multidimensional ($\geq$2) object is sampled at least twice finer than the Nyquist frequency in each dimension, the phases are uniquely encoded inside the diffraction pattern, except for some special

Manuscript received January 1, 2011; revised April 26, 2011; accepted May 14, 2011. This work was supported in part by the National Institute of Health under Grant GM081409-01A1; U.S. Department of Energy, Basic Energy Service, under the Contract DE-FG02-06ER46276; and Los Alamos National Laboratory Director's Postdoctoral Fellowship. Use of the RIKEN beamline (BL29XUL) at SPring-8 Center was supported by RIKEN, Hyogo, Japan.

J. Miao is with the Department of Physics and Astronomy and the California NanoSystems Institute, University of California, Los Angeles, CA 90095 USA (e-mail: miao@physics.ucla.edu).

R. L. Sandberg is with Physical Chemistry and Advanced Spectroscopy Group, Chemistry Division, Los Alamos National Laboratory, Los Alamos, NM 87544 USA (e-mail: sandberg@lanl.gov).

C. Song is with RIKEN SPring-8 Center, Hyogo 679-5148, Japan (e-mail: cysong@spring8.or.jp).

Color versions of one or more of the figures in this paper are available online at http://ieeexplore.ieee.org.

Digital Object Identifier 10.1109/JSTQE.2011.2157306

and trivial cases. This is synonymous with saying that, in order to make the phases retrievable, the diffraction pattern has to be oversampled finer than the inverse of the sample size at least by a factor of 2 in each dimension. In 1998, Miao *et al*. demonstrated that it is unnecessary to oversample the diffraction pattern by twice in each dimension for successful phase retrieval of 2-D and 3-D objects [9]. Based on numerical experiments of both noise-free and noisy data, they proposed that when the number of measured independent (i.e., non-centro-symmetrical) intensity points is more than the number of unknown variables, the phases can in principle be retrieved from diffraction intensities alone [9], [75]. This was later confirmed by experimental results [76]. Therefore, the conclusion by Bruck, Sodin, Hayes, and Bates is overly restrictive and only represents a subclass of the general solution to the noncrystallographic phase problem. To quantify the phase-retrieval method, a parameter termed the oversampling ratio σ was introduced [9], as shown (1) at the bottom of this page.

When $\sigma > 2$, the number of measured independent intensity points is more than the number of unknown variables, and noncrystallographic phase problem is in principle solvable in 2-D and 3-D cases [9], [75].

To retrieve the phases from the oversampled diffraction patterns, Fourier-based iterative algorithms have been widely used [10]–[16]. These algorithms typically include the following four steps. 1) A random phase set is combined with the measured Fourier modulus (i.e., square root of the diffraction intensity). By applying the inverse fast Fourier transform (FFT), a real-space image is obtained. 2) A support is defined for the image: the electron density outside the support and the negative electron density inside the support are pushed close to zero, and an updated image is obtained. 3) The Fourier modulus and phases are calculated by applying the FFT to the updated image and the new Fourier modulus is replaced with the measured one, while the new phases remain unchanged. 4) An updated image is obtained by applying the inverse FFT to the assembled Fourier modulus and phases. During this process, an error metric is used to monitor the convergence of the iterative algorithm, defined as the total electron density outside the support divided by the total density inside the support, or the difference between the measured and calculated Fourier modulus. The algorithm is terminated when no further improvement can be made. To date, a number of iterative algorithms have been developed, including the hybrid input–output [10], [11], error reduction [10], [11], difference map [12], guided hybrid input–output [13], shrink wrap [14], hybrid projection reflection [15], and relaxed averaged alternating reflectors [16].

III. CDI Methods

Although the principle of CDI is simple and elegant, the experimental realization of CDI faced several obstacles. First, compared to the diffraction intensity of a sizable crystal, the diffraction pattern of a noncrystalline specimen or a nanocrystal has a much weaker intensity distribution. Second, the incident beam has to be coherent and the coherence length required is related to the oversampling ratio of the diffraction pattern [9], [19]. Third, compared to the real-space image, the diffraction intensity has a much larger dynamic range (typically spanning a few orders), making the data acquisition a challenging task. Fourth, in order to measure high-quality diffraction patterns, area detectors with both a high dynamic range and high quantum efficiency are required. Fifth, as the intensity of the direct beam is much higher than the diffracted intensity, a beamstop has to be used to block the direct beam. The missing intensity at the center due to the beamstop represents the low-frequency information, and is critical to the phase-retrieval process. Finally, although the oversampling method with iterative algorithms works well for simulated data, it is more difficult for experimental data due to the presence of different sources of noise.

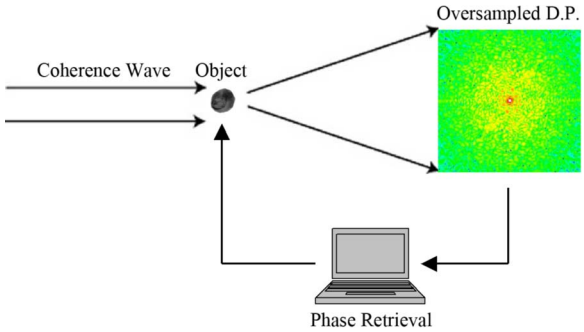

Fig. 1. Principle of CDI where a coherent wave illuminates an object and the oversampled diffraction pattern is measured by an area detector. An image is reconstructed from the diffraction pattern by using an iterative algorithm.

Notwithstanding these challenges, in 1999 Miao and colleagues made several experimental advancements to overcome these obstacles [8]. To generate a coherent incident beam, they inserted a 10 μm pinhole in front of the sample at an undulator beamline tuned to a wavelength of 1.7 nm at the National Synchrotron Light Source. The diffraction patterns were measured by a back-thinned, liquid-nitrogen-cooled charge-coupled device (CCD) camera that has high quantum efficiency at these wavelengths and very low read-out noise. To enhance the dynamic range and the signal-to-noise ratio of the diffraction pattern, they accumulated a large number of patterns at the same sample orientation and then summed them up. To overcome the missing center problem, they used an optical microscope (low-resolution) image of the specimen, and filled in the missing intensity with the Fourier modulus calculated from the low-resolution optical image. Note that the missing center problem was later solved without the need of lower resolution images [25].

Fig. 1 shows the principle of CDI, where a coherent wave illuminates an object, and an oversampled diffraction pattern of the object is measured by an area detector such as a CCD or a

$$\sigma = \frac{\text{volume of electron density region} + \text{volume of no} - \text{density region}}{\text{volume of electron density region}}. \quad (1)$$

pixilated array detector. By using iterative algorithms described earlier, the structure of the object is reconstructed from the diffraction pattern. Over the past few years, CDI has evolved into different methods which we classify here for convenience of discussion into four broad categories. The first is denoted plane-wave CDI, in which a plane wave illuminates a finite object and the far-field diffraction pattern is measured [8]. The oversampling ratio of the diffraction pattern is determined by the wavelength of the incident beam, the sample size, the distance between the sample and the detector, and the detector pixel size [9], [76]. In order to obtain a 3-D dataset, the sample has to be rotated around a tilt axis and a sequence of 2-D diffraction patterns measured at different sample orientations. Compared to other methods, plane-wave CDI has the following advantages. 1) As long as the sample is kept within the illumination area, the method is insensitive to sample vibration. 2) It is relatively straightforward to acquire 3-D datasets and perform 3-D image reconstructions. 3) The diffraction intensity from the sample is not contaminated by Poisson noise in both the direct beam and the diffraction intensity from upstream optics as the direct beam is blocked by a beamstop and the diffraction from the optics is mostly removed by a pair of corners with beveled edges [77]. 4) It can be implemented in single-shot experiments with intense coherent X-ray sources. This may explain why plane-wave CDI has achieved the highest spatial resolution ($\sim$2 nm) [78], [79] and has thus far been applied to determine most of the 3-D structures [19], [25], [28], [30], [35], [39], [40]. The main drawback of this method is the requirement of isolated objects.

The second method is termed scanning or ptychographic CDI [31], [32], [42], [44], in which a circular aperture or focusing optics is used to define an illumination probe. By scanning the sample across the illumination probe, a sequence of 2-D diffraction patterns is acquired with each pattern overlapping with its neighboring ones. This overdetermination, i.e., increasing the number of the measured intensity points than the unknown variables [9], can improve the convergence of the phase-retrieval process. The advantages of scanning CDI lie in 1) its applicability to extended objects; 2) the reconstruction of both the probe and the object simultaneously; and 3) the fast convergence of the algorithm. Compared to plane-wave CDI, however, scanning CDI has the following drawbacks: 1) each projectional image in a 3-D dataset requires a 2-D scan of the X-ray probe and any sample vibration may degrade the 3-D resolution; 2) for weak scatters such as biological samples, the high-resolution signal from the sample may be contaminated by the Poisson noise in the illumination probe; and 3) the interaction between the probe and the sample along the beam direction and the curvature of the Ewald sphere make the 3-d reconstruction become more challenging especially at high resolution.

The third method, denoted Bragg CDI [18], [20], [26], [38], [63], is mainly used for structure studies of nanocrystals. When a coherent X-ray wave illuminates a nanocrystal, the diffraction intensity distribution at each Bragg reflection is related to the shape function of the nanocrystal and the strain inside the nanocrystal. If multiple diffraction patterns around a Bragg reflection are acquired, both the 3-D shape function and the internal strain field of the nanocrystal can be obtained. With the measurement of three or four Bragg peaks, the full strain tensor can be determined. Compared to other CDI methods, Bragg CDI is unique in that it enables us to determine the 3-D the strain tensor and ion displacement inside nanocrystals at the nanometer scale resolution.

The fourth method is called Fresnel CDI (FCDI) [27], in which a focusing optics such as a zone plate is used to create a curved wave front to illuminate a sample. The illumination function of the probe needs to be retrieved beforehand in order to image the sample. A detector measures two types of patterns from the sample: a diffraction pattern at higher scattering angles and an interference pattern or hologram at lower scattering angles. The hologram is formed by the interference between the curved incident wave (which has expanded after being focused) and the scattered wave from the sample. The two patterns can be combined into a single pattern for the retrieval of the sample structure at high resolution. The main advantages of this method are 1) its rapid convergence due to the curvature of the incident wave and 2) the ability to image a subregion in an extended sample with a single view. On the other hand, FCDI requires that the sample be very stable relative to the incident beam. Recently, FCDI has also been applied to the scanning of a continuous sample [29], [80]. This technique, called keyhole diffractive imaging, adds advantages in that the field of view can be zoomed in or out by changing the position of the sample with respect to the beam focus.

IV. Applications With Synchrotron Radiation

The four CDI methods described in Section III have been widely used to image and characterize materials and biological samples [18]–[53]. To date, most of the CDI experiments have been performed on third-generation synchrotron radiation facilities. Here, we present a few examples to illustrate the power, the unique capabilities, and the potential of CDI.

A. Revealing the GaN–Ga_2O_3 Core Shell Structures in 3-D

GaN and the related wide band gap III–V nitride semiconductors have broad applications in electronic and optical device such as blue/green lasers and flat panel displays [81]. The ability to characterize the 3-D morphology and the 3-D internal structure of the nitride semiconductor materials at the nanometer scale is important to further our understanding of those materials and their functions. Plane-wave CDI has been used to perform 3-D imaging of GaN quantum dot particles [25], [28], which was heat-treated in a flowing stream of pure N_2 gas at 900 °C for 24 h. A set of 31 oversampled X-ray diffraction patterns were collected from a single GaN nanoparticle using an undulator beamline at SPring-8 with 5 keV X-rays. Phase retrieval of the diffraction patterns was conducted by the guided hybrid input–output (GHIO) algorithm [13], and 3-D image reconstruction was computed by the equally sloped tomography (EST) method [82]–[85]. Compared to Fourier-based 3-D phase retrieval [19], [35], [39], the combination of 2-D phase retrieval

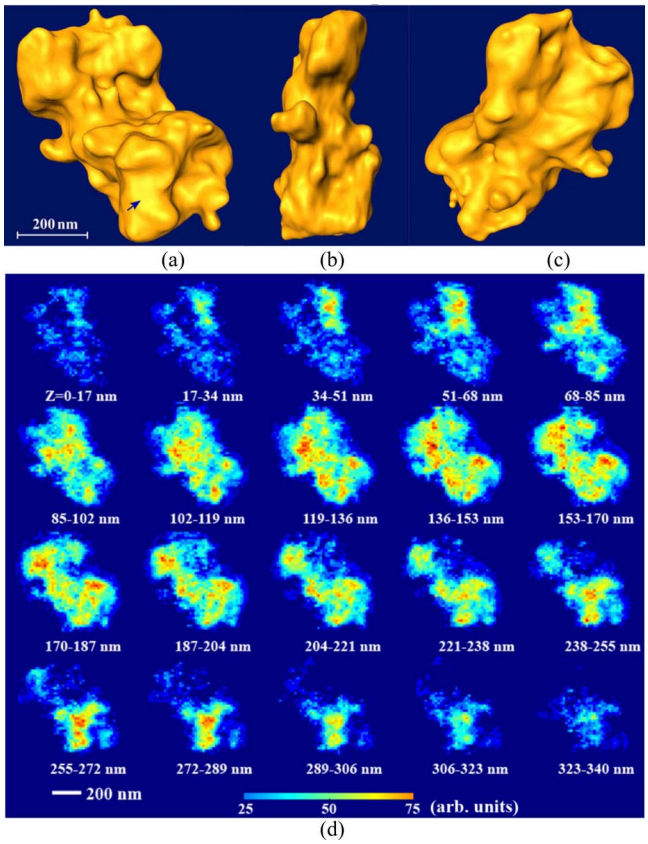

Fig. 2. Isosurface renderings of a reconstructed GaN quantum dot nanoparticle, showing (a) front view, (b) back view, and (c) side view. The platelet-like structures and the formation of small islands on the surface of the particles are visible (d) 3-D internal structure of the GaN quantum dot particle, where the z-axis is perpendicular to (a) front view and points outward. The 3-D GaN-Ga_2O_3 core shell structure is clearly visible where the low electron density corresponds to β-Ga_2O_3 and the high density corresponds to the GaN cores. [28].

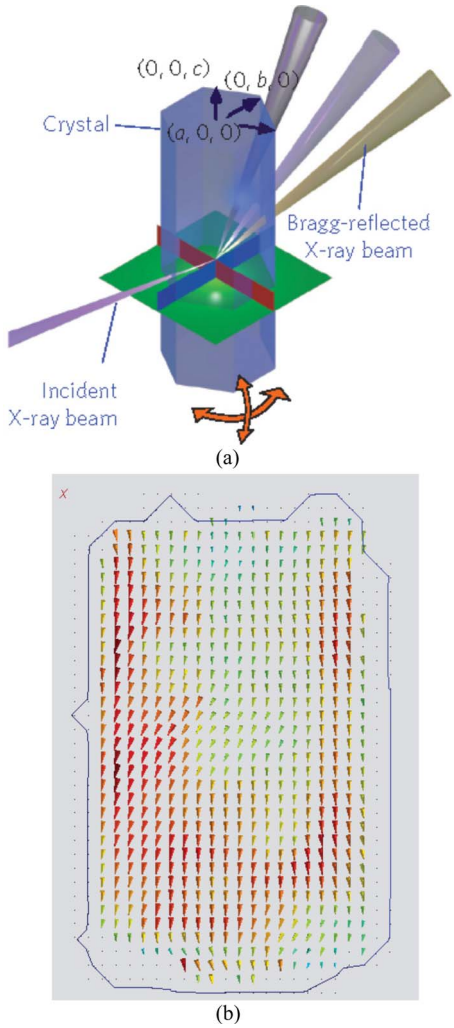

Fig. 3. (a) Schematic layout of Bragg CDI with multiple Bragg reflections from a ZnO rod. (b) Slice of the reconstructed 3-D ion displacement field inside the ZnO rod in which the direction of each arrow indicates the direction of the displacement and the size of each arrow indicates the magnitude of the displacement. [38].

with EST has proved to be more effective when there is a limited number of diffraction patterns [28], [40].

Fig. 2 shows the reconstructed 3-D image of the GaN nanoparticle, where Fig. 2(a)–(c) represent the front, the side, and the back view of the particle, respectively. A distinctive feature of the particle is the platelet-like structures and the formation of small islands on the surface of the particle due to the surface oxidation of GaN platelets after the heat treatment. Fig. 2(d) shows 20 slices with each slice of 17 nm thick, sectioning through the GaN nanoparticle. The colors in the slices represent the different electron density: red represents the higher density, yellow the medium density, and blue the lower density. Fig. 2(d) shows that the higher density—concentrated near the center of the platelets—is surrounded by the lower density. It was concluded that the lower density is β-Ga_2O_3 and the higher density GaN [28]. The observation of the 3-D internal structures of the heat-treated GaN particles provides the direct evidence of the existence of GaN–Ga_2O_3 core shell structures, which is not easily accessible by other imaging techniques.

B. 3-D Imaging of Strain Inside Nanocrystals

The ability of 3-D imaging of the ion displacement and strain inside nanocrystals has important implications in designing future materials and making new devices. Bragg CDI, pioneered by Robinson *et al*. in 2001 [18], offers the unique capability of mapping out the full strain tensor inside nanocrystals at nanometer scale resolution. Fig. 3(a) shows a schematic layout of Bragg CDI with multiple Bragg reflections from a single ZnO rod [38]. The experiment was conducted at the Advanced Photon Source using a wavelength of 1.42 Å. By carefully rotating the ZnO rod, oversampled X-ray diffraction patterns were measured at six Bragg reflection directions, which are related to both the shape function of the rod and the strain inside the rod. By using the iterative algorithm described in Section II, the diffraction patterns were inverted into two parts: the reconstructed magnitudes and phases. While the reconstructed magnitudes correspond to the shape of the rod, the phases are related to the 3-D ion displacement inside the rod. This ion displacement information can be

used to construct the strain tensor. Fig. 3(b) shows a slice of the 3-D ion displacement field inside the ZnO rod in which the direction of each arrow indicates the direction of the displacement and the size of each arrow indicates the magnitude of the displacement [38]. Although the resolution of Bragg CDI is currently around 40 nm, utilization of more brilliant X-ray sources will be able to significantly improve its spatial resolution.

C. Quantitative 3-D Imaging of a Yeast Spore Cell

Cryoelectron tomography is the method of choice for high-resolution 3-D imaging of biological structures, but it is only applicable to thin or sectioned specimens (typically $\leq 0.5\ \mu$m) [86], [87]. Compared to electrons, X-rays have a longer penetration depth and can be used to image thicker biological samples. However, X-rays are more difficult to focus [88]. For biological specimens, the highest resolution achievable using lens-based X-ray microscopy is around 30–50 nm [89]. One way to overcome the resolution limitation is to employ CDI. Over the past few years, CDI has been applied to image whole cells, cellular organelles, viruses, and biomaterials [21], [24], [30], [33]–[37], [40]–[42], and a highest resolution of 10–15 nm has been achieved on biological samples [41].

Here, we illustrate an example on 3-D quantitative imaging of a *Schizosaccharomyces pombe* yeast spore cell [40]. The spore cells were fixed with formaldehyde and glutaraldehyde and then air-dried. By tilting a yeast spore cell along a rotation axis, a series of 25 X-ray diffraction patterns were measured. The limited number of diffraction patterns is due to the concern of radiation damage to the sample. The phase retrieval and 3-D image reconstruction were performed by using the GHIO algorithm [13] and the EST method [82]–[85]. Fig. 4(a) shows a volume rendering of the reconstructed 3-D image, in which the nucleus is in orange, the endoplasm reticulum (ER) in green, the vacuole in white, the mitochondria in blue, and the granules are in light blue. Fig. 4(b) shows a zoomed view of the mitochondria, the ER, and the nucleus. The mitochondria with an elongated shape have relatively high density. The network-like structure of the ER, composed of fibril-like structure connecting the nucleus and the spore membrane, was visualized. The nucleus has a high density, and a region near the center of the nucleus has the highest density in the cell, which is likely the nucleolus [see Fig. 4(b) inset]. Fig. 4(c) shows the 3-D structure of the vacuole with an irregular 3-D morphology. The cross-sectional image (see Fig. 4(c), inset) indicates the existence of high-density spots inside the vacuole, which may be vacuolar granules and aggregation of proteins. A thin slice of the reconstructed yeast spore and a line scan across the slice are illustrated in Fig. 4(d) and (e), respectively, showing the density variation across a mitochondrion and the vacuole. This experiment indicates the potential of quantitative 3-D imaging of a wide range of cells and cellular structures at nanometer-scale resolutions that are too thick for electron microscopy.

D. Imaging of a Frozen Hydrated Yeast Cell

By avoiding the use of lenses, CDI overcomes the resolution barrier set by the X-ray optics. For biological specimens, the resolution of CDI is ultimately limited by radiation damage to the specimens [90]. Using cryogenic technologies, the radiation damage effect can be mitigated, and a 3-D resolution of 5–10 nm is likely achievable [91], [92].

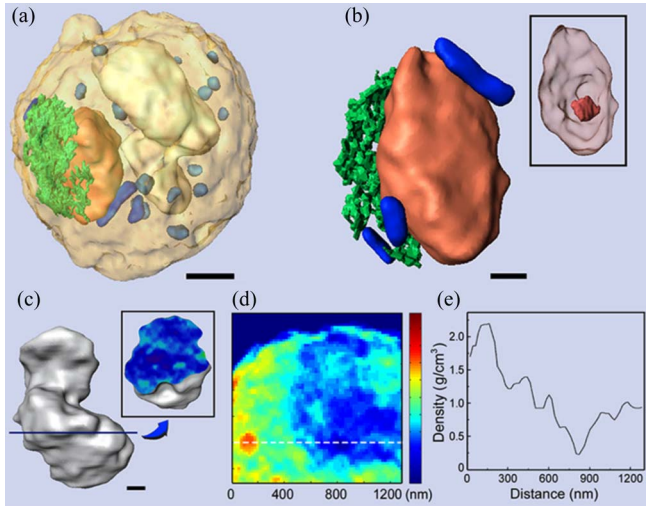

Fig. 4. 3-D quantitative imaging of a *Schizosaccharomyces pombe* yeast spore cell. (a) Volume rendering of the reconstructed yeast spore, showing nucleus (orange), ER (green), vacuole (white), mitochondria (blue), and granules (light blue). Scale bar is 500 nm. (b) Zoomed view of the 3-D morphology and structure of the nucleus, ER, and mitochondria. Inset shows the nucleolus (orange). Scale bar is 200 nm. (c) 3-D morphology and structure of the vacuole. Inset shows a cross-sectional image of the vacuole. Scale bar is 200 nm. (d), (e) A thin slice of the reconstructed yeast spore and a line scan along the dashed line, showing the density variation across a mitochondrion and the vacuole. [40]

Although the cryogenic technologies have been widely used in cryoelectron microscopy (cryo-EM) and soft X-ray microscopy, their application to CDI has recently been initiated. To date, two groups have successfully reconstructed the structure of frozen-hydrated cells: one on *D. radiodurans* bacteria [37] and the other on a *Saccharomyces cerevisiae* yeast cell [36]. Fig. 5(a) shows the differential-interference-contrast image of a yeast cell. The cells were plunge-frozen in liquid ethane to minimize ice crystal formation. X-ray diffraction patterns were measured from the frozen-hydrated yeast cells using a soft X-ray undulator beamline at the Advanced Light Source with a wavelength of 2.38 nm. A reconstructed image is shown in Fig. 5(b), which represents a projectional view of a cell. Since the cell is 3-D, the internal structure of the cell is not clearly visible in the projectional image. In order to identify the cellular organelles and other structure inside the cell, 3-D image reconstruction (described in Section IV-C) is required. Nevertheless, this experiment [36], along with the CDI experiment on *D. radiodurans* bacteria conducted at the Europe Synchrotron Radiation Facility [37], indicates that the cryogenic technologies can be used to significantly reduce the radiation damage effect in coherent X-ray diffraction imaging of biological specimens.

V. Application With Tabletop Sources: High Harmonic Generation and Soft X-Ray Lasers

While CDI has proven to be a powerful and rapidly developing technique, a limitation to further development and application

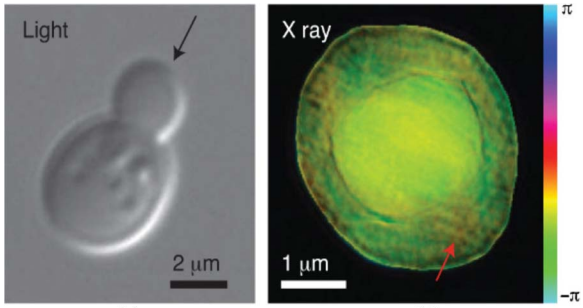

Fig. 5. Coherent diffraction image of a frozen-hydrated yeast cell. (a) Differential-interference-contrast image of a yeast cell in which the arrow indicates the assumed direction of the incident X-ray beam. (b) Reconstructed image of a frozen-hydrated yeast cell in which the red arrow indicates a possible mitochondrion. [36].

has been the availability of coherent X-ray sources. Competitive "beam time" at third-generation synchrotrons and newer free electron facilities has limited the number of groups that are currently working on the CDI techniques. This roadblock is of particular concern in potential areas of application such as cellular biology or materials science where many times it is not feasible to take necessary laboratory equipment to larger light sources. However, the past two decades have seen the emergence of bright, tabletop sources of coherent extreme ultraviolet (EUV) and soft X-ray radiation (SXR) that produce wavelengths from a few nanometers to 100 nm wavelengths [93], [94].

A. *Coherent Tabletop Soft X-Ray Sources*

Although producing radiation at longer wavelengths (1–50 nm), tabletop sources such as HHG and SXR lasers can produce as much coherent flux as undulator beamlines from third-generation synchrotron radiation sources [93]. The rapid development of tabletop short-wavelength sources has largely been brought about by the increasing pulse energy and decreasing pulse duration of commercially available ultrafast lasers. Ultrafast lasers in the optical and near-IR wavelength range with approximately 10 s of femtosecond pulse durations (10^{-14} s) and terawatt (10^{12} W) peak powers are widely available [95]. These intense laser pulses enable the processes that the most successful tabletop coherent X-ray sources utilize: nonlinear upconversion through HHG and gain in highly ionized plasmas for soft X-ray lasers [94], [96], [97].

While a wide variety of tabletop X-ray sources exist, such as simple X-ray tubes, laser plasma sources, solid-target HHG, betatron radiation, and laser-driven free-electron lasers [98]–[102], only two sources have had sufficient coherent flux to enable coherent X-ray imaging [45]–[49], [103]–[108]. Soft X-ray lasers are produced in a highly ionized, dense plasma where a population inversion, and thus gain, can occur on an ionized electronic transition (such as neon-like argon or nickel-like silver) [94], [97], [109], [110]. The plasma is created and the lasing transition is "pumped" either electrically by a fast electrical discharge through an argon filled capillary [111] or by an intense ultrafast laser irradiating a solid target [112]. These lasers can receive enough population inversion that gain saturation can be achieved in a single-pass laser geometry. While these lasers provide extreme temporal coherence (or monochromaticity) of up to $\lambda/\Delta\lambda = 10^5$, their spatial coherence is limited due to their single-pass nature with no laser cavity. However, full spatial coherence has been demonstrated by seeding the lasers with a spatially coherent source [113], [114]. Still, achieving gain saturation enables high pulse energies in nanosecond pulses (∼millijoules for 46.9 nm Ne-like Ar gas lasers and microjoules for solid target lasers with >10 nm wavelength). Due to the longer, nanosecond, pulse duration of traditional SXR lasers, truly ultrafast time-resolved CDI has not been a possibility. Another limitation of current tabletop SXR sources has been their limitation to longer wavelengths (>10 nm) due to the demanding pump power requirements that scales as $1/\lambda^4$ [94], [97].

An additional attractive tabletop source for coherent imaging is phase-matched HHG that has demonstrated full spatial and temporal coherence and scalability to shorter wavelengths (down to 1 nm) [105], [135]. HHG can be thought of as the coherent equivalent of a Roentgen X-ray tube. The nonlinear upconversion of optical or IR photons into the EUV and SXR regions is described semiclassically by a three-step model [115], [116]. First, an ultrafast intense laser incident on a gas target ionizes the gas atoms. Second, the ionized electron is accelerated away from the parent ion by the laser electric field. Finally, a half period later, the oscillating laser electric field switches direction and the electron is accelerated back toward the parent ion where it can give up the gained kinetic energy as a high-energy photon. The HHG process produces a comb of odd harmonics that can span out to the hundreds of electron volts photon energy in the so-called cutoff region. The maximum photon energy of these cutoff photons is given by

$$E_{\text{cutoff}} = h\nu = I_p + 3.2\,U_p (U_p \propto I_{\text{laser}}\lambda^2) \tag{2}$$

where h is Plank's constant, ν is the photon frequency, I_p is the ionization potential of the electron, U_p is the pondermotive energy of the accelerated electron which is proportional to the peak laser intensity I_{laser} and the square of the driving laser wavelength λ [93], [115], [116]. With enough laser intensity, cutoff photons in the 1 keV region have been observed from HHG [112], [117], [118]. However, for bright, coherent flux, the HHG process must be phase matched by adjusting the gas target pressure, laser focus (Guoy) phase, or through more exotic quasi-phase matching techniques [105], [119]–[123]. An additional attractive aspect of HHG is that it has produced the shortest optical pulses to date—subfemtosecond or attosecond pulses [124]–[127]. Additionally, Wang *et al*. demonstrated that by seeding a laser-driven SXR laser with an HHG pulse, they decreased the pulse duration and increased the spatial coherence of their SXR laser [128]. This HHG seeding produced picosecond (10^{-12} s) pulses with ∼microjoules type energies that had full spatial and temporal coherence. Thus, CDI with femtosecond or attosecond time resolution of dynamic processes becomes a possibility.

B. First Tabletop Demonstrations

With their higher pulse energies, tabletop SXR lasers were first applied to coherent X-ray imaging. Several initial applications of tabletop SXR lasers to studying plasmas in interferometers were demonstrated by Rocca *et al.* [129] a little over a decade ago. A few years later in 2002, Bartels *et al*. demonstrated full spatial coherence and moderately high-resolution coherent imaging (in-line holography) with a phase-matched high harmonic source [105]. This initial result had lower spatial resolution of about 10 μm due to the illuminating beam not being tightly focused. In 2006, demonstrations of higher resolution holography (several 100 nm to several micrometers resolution) followed with both a spatially filtered 46.9-nm capillary-discharge SXR laser and a phase-matched 32-nm HHG source [103], [130]. Coherent imaging with these tabletop SXR sources in the in-line holography geometry was limited to the numerical aperture of the scattered reference wave, which was limited to about half a micrometer. This resolution is not much better than a standard optical microscope and has been limited by the longer wavelength of soft X-ray laser sources [104]. Furthermore, with intense soft X-ray lasers, single-shot imaging with holographic [106] and zone plate techniques has been demonstrated [131]. However, by applying CDI with oversampling and iterative phase retrieval to a phase-matched 32-nm HHG source, Sandberg *et al*. were able to achieve 200 nm resolution in 2007 [45], [132].

Fundamentally, the resolution of CDI is ultimately limited by coherent flux and wavelength and not by reference beam numerical aperture as with holographic techniques. This fact was demonstrated by Sandberg *et al*. with the same phase-matched 32-nm HHG source, and with a spatially filtered 46.9-nm capillary discharge laser [46]. By focusing their coherent SXR beams more tightly (about 15 μm spot) and by placing their detector in a high numerical aperture (NA) geometry (only 17 mm from a sample to CCD), they were able to achieve sub-100 nm spatial resolution with CDI. With the 32-nm HHG source, they achieved about 90 nm resolution with an integration time of 80 min. Also, with the 46.9-nm spatially filtered SXR laser, they were able to achieve 72 nm resolution with an integration time of 5 min or 300 shots [see Fig. 6(a)]. This result was the highest NA X-ray image at the time—0.6 NA with a resolution only 1.5 times the illuminating wavelength. In the case of the HHG source, the resolution was limited by available 32 nm flux and practical integration time, whereas with the tabletop SXR source, the resolution was limited only by the size of the detector. With the same SXR laser source, but with a slightly optimized HHG source, resolutions of 50 nm were achieved by a combination of holography and phase retrieval, respectively [48], [104]. Thus, wavelength-limited resolution with bright, ultrafast, tabletop coherent SXR sources is possible. As shown in Fig. 6(b), an additional fortuitous consequence of this high NA geometry is the ability to image samples in 3-D with a single exposure angle. This technique, called ankylography, relies on the fact that high NA diffraction data lie on the curved Ewald sphere in Fourier space. By reanalyzing the 0.6 NA diffraction data from the 46.9-nm SXR laser, Raines *et al*. were able to reconstruct the stick figure sample in 3-D [49].

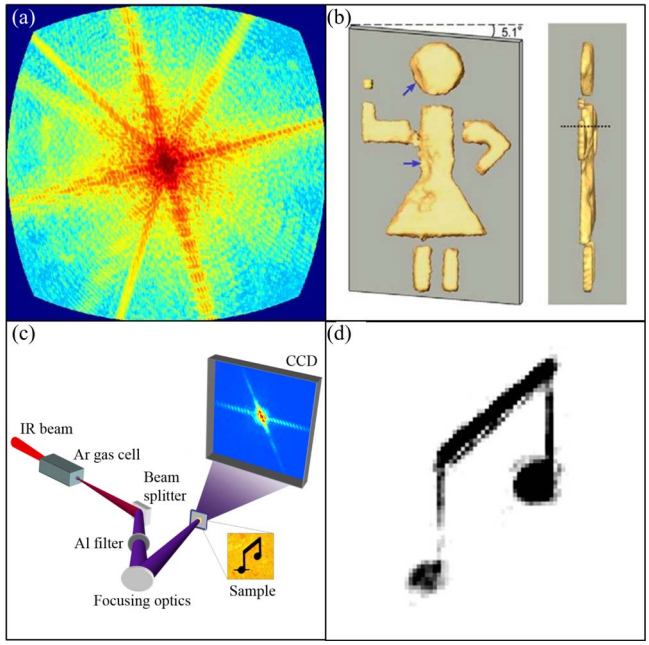

Fig. 6. (a) High NA curvature corrected diffraction data from 46.9 nm SRX laser [45]. (b) 3-D ankylographic reconstruction from a single 2-D curved diffraction pattern [49]. (c) Schematic of a single-shot HHG CDI setup [47]. (d) Single-shot reconstruction of a test sample [47].

C. Single-Shot CDI on a Tabletop

While these initial applications of CDI to tabletop sources proved the ability to achieve wavelength-limited resolution, the practicality of the technique has been limited by two factors: integration time and wavelength. First, CDI with kilohertz repetition rates has, to this point, been limited to microwatt powers in a single harmonic, thus requiring minutes to hours of integration to achieve near-wavelength-limited resolution. Consequently, hundreds of thousands to millions of pulses must be integrated to achieve sufficient signal to noise at high scattering angles in order to obtain wavelength-limited resolution. For applications in time-resolved imaging, this limits CDI to repetitive processes in a pump–probe stroboscopic experiment. However, HHG can produce much higher pulse energies if it is driven with higher laser pulse energies. This fact was demonstrated recently by Ravasio *et al*. on a larger laser system with 50 mJ, 20 fs pulses. This laser produced enough phase-matched coherent HHG light at 32 nm (about 1 μJ or $10^{1}1$ photons) in a single femtosecond pulse to achieve near 100 nm resolution in a single shot [see Fig. 6(d)] and 60 nm resolution with multiple pulses [47], [133]. This single-shot CDI with femtosecond HHG pulses, like single-shot imaging at XFELs [50], opens many possibilities: imaging nonreversible processes, collecting a single image before radiation damage takes place, etc.

While this result clearly illustrates the potential power of CDI with femtosecond pulses from tabletop sources, all current CDI on tabletop sources has been limited to illuminating wavelengths of 10 s of nanometers or longer. These wavelengths are readily absorbed in almost all materials thus limiting its usefulness to potential applications. Recently, however, HHG

driven with longer, mid-IR wavelengths of 1–2 μm has produced bright, phase-matched and spatially coherent X-rays up to 500 eV photon energy [134]–[136]. These photon energies span the biologically important water window [94] and may possibly extend bright coherent HHG to the 1 nm wavelength range. Thus, in coming years, HHG with CDI may provide single-shot, near-wavelength-limited resolution of femtosecond (or attosecond) dynamics across numerous soft X-ray absorption edges in such applications as cellular biology, dynamics of magnetic domains in storage media, or heat transport at interfaces and in nanomaterials [137], [138]

VI. Application With X-Ray Free-Electron Lasers

Although CDI removes the need of sample crystallinity, the resolution currently attainable is far lower than that of crystallography, which is mainly due to the loss of the amplification from a large number of unit cells inside a crystal ($\sim 10^{15}$ in a typical protein crystal). The highest resolution thus far achieved in CDI is $\sim$2 nm for inorganic materials and $\sim$10–20 nm for biological specimens [41], [79]. To improve the resolution of CDI and compensate the loss of the large number of the unit cells, more brilliant X-ray sources are needed. However, increasing the incident X-ray flux means depositing more energy in the specimen, which results in the breaking of chemical bonds and discharging of binding electrons. This irrecoverable radiation damage effect ultimately limits the resolution in CDI [91], [92].

One way to alleviate the radiation damage effect is to use very short X-rays pulses [139], [140]. Numerical simulation studies by Neutze *et al*. suggested that when an intense X-ray pulse is shorter than 10 fs and illuminates a biomolecule, a diffraction pattern may be recorded from the molecule before it is destroyed by the pulse [140]. The combination of intense and ultrashort X-ray pulses with CDI, hence, may allow structural determination of single biomolecules without the need of crystallization [141]. To obtain the 3-D structure of single biomolecules, many identical copies of the molecules are needed. Numerical simulations suggested that, with about 10^6 identical copies, a resolution of 2.5 Å may be achievable for large protein molecules [141]. This method (termed single-particle CDI) potentially opens a new horizon for 3-D structural determination of biomolecules, but requires an entirely new type of coherent X-ray source—an X-ray free-electron laser (XFEL).

A. X-Ray Free-Electron Lasers

XFELs are able to produce X-ray pulses with a peak brilliance a billion times higher than the brightest synchrotron radiation source currently available. In a synchrotron radiation source, electron bunches circulate in a storage ring and produce X-rays at designated linear or bending sections. In an XFEL, very compact and high-density electron bunches travel through a long undulator to produce intense and short X-ray pulses. Initially, the electron bunches emit incoherent radiation because the size of the electron bunches is larger than the wavelength of the radiation. If the undulator magnet array is tuned precisely to match the phase and wavelength of the radiation, the radiation modulates the electrons and produces a process called "microbunching,"

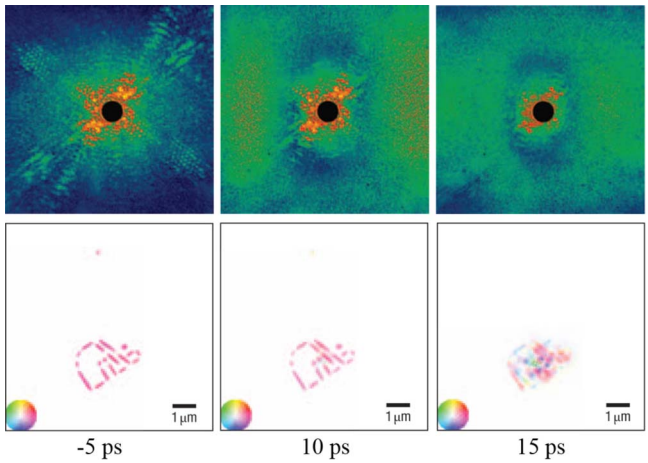

Fig. 7. Ultrafast CDI of a laser ablation process on etched patterns in Si3N4 membranes. A high-power visible laser, synchronized with EUV-FEL from FLASH, was employed to ablate the pattern and the EUV-FEL pulse was used as a probe to image the ablated specimen [51].

which exponentially amplifies the intensity of the radiation. After the electron bunches travel a certain distance, the amplification becomes saturated and the electron beam is dumped. This process, called self-amplified spontaneous emission [142], produces radiation with full transverse coherence, high peak intensity ($\sim 10^{12}$ photons/pulse), and short pulse duration ($\sim$tens to hundreds of femtoseconds).

Presently, several X-ray and EUV FEL facilities are in operation, including the LCLS, Stanford, U.S.; the FLASH, DESY, Germany; and the SCSS, SPring-8, Japan [143]–[145]. In addition, two more XFEL facilities are expected to operate within the next few years: the Japanese XFEL (SPring-8) in 2011 and the European XFEL (DESY) in 2016.

B. Ultrafast CDI

The feasibility of CDI with an intense, short-pulsed FEL has been demonstrated by Chapman *et al*. at the FLASH [50]. They recorded the diffraction pattern of a test pattern by using a single-intense FEL pulse before it was destroyed by the pulse. An image was then retrieved from the single-shot diffraction pattern. The experiment has also demonstrated CDI's inherent potential as an ultrafast imaging technique. Later, the ultrafast imaging capability of CDI was demonstrated through a time-resolved, pump–probe experiment (see Fig. 7) [51]. The experiment employed 10 fs FEL pulses from the FLASH. A high-power, pulsed optical laser was used to ablate a patterned specimen on a Si_3N_4 membrane. The EUV-FEL light was used as a probe to image the sample with a controlled time delay by synchronizing the two sources. While this proof-of-concept ultrafast CDI experiment achieved a temporal resolution of $\sim$10 ps, the resolution will likely be improved down to the femtosecond level in the future.

C. Single-Particle CDI

Among all the potential applications of CDI, single-particle CDI is arguably the most challenging one due to the following reasons. First, the scattering intensity of an XFEL pulse

by a single biomolecule is extremely weak. Second, compared to electrons, the scattering cross section of X-rays with atoms is ∼five to six orders lower. Thus, electrons in principle have advantages over X-rays for structural determination of small particles. On the other hand, X-rays do not have the charging effect and XFELs can produce intense X-ray pulses with $\sim 10^{12}$ photons per pulse [143]–[145], which is far more than an electron pulse can produce. Also, the short pulse duration of XFELs potentially allows acquisition of the diffraction pattern from a biomolecule before it is destroyed [140]. In order to obtain the 3-D structural information, many identical copies of biomolecules (typically on the order of 10^6) have to be injected into an XFEL beam at random orientations [141]. Those hit by the XFEL pulses will generate very weak 2-D diffraction patterns. To enhance the signal to noise ratio of the diffraction intensity, sophiscated algorithms are needed to align and average the large number of weak diffraction patterns [146]–[150], which is similar to the methods developed in single-particle cryo-EM [151]. After postanalysis, the diffraction patterns can then be assembled into a 3-D pattern and phased to obtain the 3-D structure of the biomolecules [141], [152], [153]. Although single-particle CDI has been mainly studied by using numerical simulations thus far, two experiments were conducted on single virus particles. The first was on the imaging of an unstained herpesvirus virion at a resolution of 22 nm by using SPring-8 [33]. The other was on the imaging of single mimiviruses at 32 nm resolution with the LCLS [154]. In the latter case, the phase retrieval was not so stable because the missing center of the diffraction pattern is larger than the centrospeckle [25]. While encouraging results have been obtained in both numerical simulations and preliminary experiments, several important questions on single-particle CDI have to be answered by future experiments: whether near atomic or atomic resolution of single biomolecules can be experimentally achieved with CDI; what the smallest size of biomolecules can be studied by single-particle CDI; and whether single-particle CDI can compete with single-particle cryo-EM.

Another potentially important direction is the newly developed ankylography technique, where the 3-D structure of a small object (or a large object at lower resolution) can in principle be determined from a single 2-D diffraction pattern sampled on the Ewald sphere [49]. Compared to single-particle CDI, ankylography has limited spatial resolution and is probably only applicable to certain classes of specimens. However, the main advantage of ankylography lies in its ability to perform 3-D structural determination from a single particle without the necessity of averaging. As ankylography remains a very preliminary approach, more work is needed to understand its potential applications and limitations. For those who are interested in ankylography, the basic ankylographic reconstruction codes have been posted on a public website, and can be freely downloaded and tested [155].

VII. Conclusion

Since its first experimental demonstration about a decade ago [8], CDI has undergone rapid development. Novel methods have been demonstrated and new applications in biology and materials/nanoscience have been pursued. To date, most of the CDI work has been conducted on third-generation synchrotron radiation sources [8], [18]–[44], and a highest resolution of ∼2 nm has been achieved at SPring-8 [79]. For materials science samples, it is anticipated that subnanometer and even atomic resolution may be achievable in the future. For biological samples, radiation damage ultimately limits the resolution of CDI. By using cryogenic technologies, the radiation damage effect can be mitigated and a 3-D resolution of 5–10 nm will likely be attainable [91], [92]. Another way to reduce the radiation damage effect is to use ultrashort X-ray pulses [140]. As femtosecond XFELs are currently under rapid development worldwide, CDI will soon enter a new frontier for high-resolution structure studies at a femtosecond time scale. Compared to scanning probe microscopy [5] and electron microscopy [4], CDI can be applied to image thick objects at high resolution in 3-D. However, currently a major limitation in CDI is the lack of tabletop coherent X-ray sources. As SXR lasers and HHG sources at the X-ray regime are under active development worldwide, it is foreseeable that CDI will be available in individual laboratories in the near future. Looking forward, CDI research within the next decade will be surely more exciting than the past one.

Acknowledgment

The authors would like to thank their wonderful collaborators, including T. Ishikawa, M. M. Murnane, H. C. Kapteyn, H. Jiang, C.-C. Chen, R. Xu, K. S. Raines, B. P. Fahimian, S. Salha, J. Rodriguez, L. Rong, J. J. Rocca, B. F. Schlotter, Y. Kohmura, Y. Nishino, T. K. Lee, F. Tamanoi, S. Risbud, and R. Sun.

References

[1] S. M. Hurtley and L. Helmuth, "The future looks bright," *Science*, vol. 300, p. 75, 2003.
[2] K. I. Willig *et al.*, "STED microscopy reveals that synaptotagmin remains clustered after synaptic vesicle exocytosis," *Nature*, vol. 440, pp. 935–939, 2006.
[3] E. Betzig *et al.*, "Imaging intracellular fluorescent proteins at nanometer resolution," *Science*, vol. 313, pp. 1642–1645, Sep. 2006.
[4] J. Spence, *High-Resolution Electron Microscopy*. New York: Oxford Univ. Press, 2003.
[5] W. A. Hofer *et al.*, "Theories of scanning probe microscopes at the atomic scale," *Rev. Modern Phys.*, vol. 75, pp. 1287–1331, 2003.
[6] A. Sakdinawat and D. Attwood, "Nanoscale X-ray imaging," *Nat. Photon.*, vol. 4, pp. 840–848, 2010.
[7] H. Mimura *et al.*, "Breaking the 10 nm barrier in hard-X-ray focusing," *Nat. Phys.*, vol. 6, pp. 122–125, 2010.
[8] J. Miao *et al.*, "Extending the methodology of X-ray crystallography to allow imaging of micrometer-sized non-crystalline specimens," *Nature*, vol. 400, pp. 342–344, 1999.
[9] J. Miao *et al.*, "Phase retrieval from the magnitude of the Fourier transforms of nonperiodic objects," *J. Opt. Soc. Amer. A*, vol. 15, pp. 1662–1669, 1998.
[10] J. R. Fienup, "Reconstruction of an object from the modulus of its Fourier transform," *Opt. Lett*, vol. 3, pp. 27–29, 1978.
[11] J. R. Fienup, "Phase retrieval algorithms: a comparison," *Appl. Opt.*, vol. 21, pp. 2758–2769, 1982.
[12] V. Elser, "Solution of the crystallographic phase problem by iterated projections," *Acta Crystallogr. A*, vol. 59, pp. 201–209, 2003.
[13] C. C. Chen *et al.*, "Application of optimization technique to noncrystalline X-ray diffraction microscopy: Guided hybrid input–output method," *Phys. Rev. B*, vol. 76, p. 064113, 2007.
[14] S. Marchesini, "A unified evaluation of iterative projection algorithms for phase retrieval," *Rev. Sci. Instrum.*, vol. 78, p. 011301, 2007.

[15] H. H. Bauschke *et al.*, "Hybrid projection-reflection method for phase retrieval," *J. Opt. Soc. Amer. A*, vol. 20, pp. 1025–1034, 2003.

[16] D. R. Luke, "Relaxed averaged alternating reflections for diffraction imaging," *Inverse Problems*, vol. 21, pp. 37–50, 2005.

[17] D. Sayre, *Imaging Processes and Coherence in Physics*. (Springer Lecture Notes in Physics, vol. 112). New York, Berlin: Springer-Verlag, 1980, pp. 229–235.

[18] I. K. Robinson *et al.*, "Reconstruction of the shapes of gold nanocrystals using coherent X-ray diffraction," *Phys. Rev. Lett.*, vol. 87, p. 195505, 2001.

[19] J. Miao *et al.*, "High resolution 3D X-ray diffraction microscopy," *Phys. Rev. Lett.*, vol. 89, p. 088303, 2002.

[20] G. J. Williams *et al.*, "Three-dimensional imaging of microstructure in Au nanocrystals," *Phys. Rev. Lett.*, vol. 90, p. 175501, 2003.

[21] J. Miao *et al.*, "Imaging whole Escherichia coli bacteria by using single-particle X-ray diffraction," *Proc. Na. Acad. Sci. USA*, vol. 100, pp. 110–112, 2003.

[22] S. Marchesini *et al.*, "X-ray image reconstruction from a diffraction pattern alone," *Phys. Rev. B*, vol. 68, p. 140101, 2003.

[23] K. A. Nugent *et al.*, "Unique phase recovery for nonperiodic objects," *Phys. Rev. Lett.*, vol. 91, p. 203902, 2003.

[24] D. Shapiro *et al.*, "Biological imaging by soft X-ray diffraction microscopy," *Proc. Nat. Acad. Sci. USA*, vol. 102, pp. 15343–15346, 2005.

[25] J. Miao *et al.*, "Quantitative image reconstruction of GaN quantum dots from oversampled diffraction intensities alone," *Phys. Rev. Lett.*, vol. 95, p. 085503, 2005.

[26] M. A. Pfeifer *et al.*, "Three-dimensional mapping of a deformation field inside a nanocrystal," *Nature*, vol. 442, pp. 63–66, 2006.

[27] G. J. Williams *et al.*, "Fresnel coherent diffractive imaging," *Phys. Rev. Lett.*, vol. 97, p. 025506, 2006.

[28] J. Miao *et al.*, "Three-dimensional GaN–Ga_2O_3 core shell structure revealed by X-ray diffraction microscopy," *Phys. Rev. Lett.*, vol. 97, p. 215503, 2006.

[29] B. Abbey *et al.*, "Keyhole coherent diffractive imaging," *Nat. Phys.*, vol. 4, pp. 394–398, 2008.

[30] H. Jiang *et al.*, "Nanoscale imaging of mineral crystals inside biological composite materials using X-ray diffraction microscopy," *Phys. Rev. Lett.*, vol. 100, p. 038103, 2008.

[31] J. M. Rodenburg *et al.*, "Hard-X-ray lensless imaging of extended objects," *Phys. Rev. Lett.*, vol. 98, p. 034801, 2007.

[32] P. Thibault *et al.*, "High-resolution scanning X-ray diffraction microscopy," *Science*, vol. 321, pp. 379–382, 2008.

[33] C. Song *et al.*, "Quantitative imaging of single, unstained viruses with coherent X rays," *Phys. Rev. Lett.*, vol. 101, p. 158101, 2008.

[34] G. J. Williams *et al.*, "High-resolution X-ray imaging of plasmodium falciparum-infected red blood cells," *Cytometry Part A*, vol. 73, pp. 949–957, 2008.

[35] Y. Nishino *et al.*, "Three-dimensional visualization of a human chromosome using coherent X-ray diffraction," *Phys. Rev. Lett.*, vol. 102, p. 018101, 2009.

[36] X. Huang *et al.*, "Soft X-ray diffraction microscopy of a frozen hydrated yeast cell," *Phys. Rev. Lett.*, vol. 103, p. 198101, 2009.

[37] E. Lima *et al.*, "Cryogenic X-ray diffraction microscopy for biological samples," *Phys. Rev. Lett.*, vol. 103, p. 198102, 2009.

[38] M. C. Newton *et al.*, "Three-dimensional imaging of strain in a single ZnO nanorod," *Nat. Mater.*, vol. 9, pp. 279–279, 2010.

[39] Y. Takahashi *et al.*, "Three-dimensional electron density mapping of shape-controlled nanoparticle by focused hard X-ray diffraction microscopy," *Nano Lett.*, vol. 10, pp. 1922–1926, 2010.

[40] H. Jiang *et al.*, "Quantitative 3D imaging of whole, unstained cells by using X-ray diffraction microscopy," *Proc. Nat. Acad. Sci.*, vol. 107, pp. 11234–11239, 2010.

[41] J. Nelson *et al.*, "High-resolution X-ray diffraction microscopy of specifically labeled yeast cells," *Proc. Nat. Acad. Sci.*, vol. 107, pp. 7235–7239, Apr. 2010.

[42] K. Giewekemeyer *et al.*, "Quantitative biological imaging by ptychographic X-ray diffraction microscopy," *Proc. Nat. Acad. Sci.*, vol. 107, pp. 529–534, 2010.

[43] J. Gulden *et al.*, "Coherent X-ray imaging of defects in colloidal crystals," *Phys. Rev. B*, vol. 81, p. 224105, 2010.

[44] M. Dierolf *et al.*, "Ptychographic X-ray computed tomography at the nanoscale," *Nature*, vol. 467, pp. 436–439, 2010.

[45] R. L. Sandberg *et al.*, "Lensless diffractive imaging using tabletop coherent high-harmonic soft-X-ray beams," *Phys. Rev. Lett.*, vol. 99, p. 098103, 2007.

[46] R. L. Sandberg *et al.*, "High numerical aperture tabletop soft X-ray diffraction microscopy with 70-nm resolution," *Proc. Nat. Acad. Sci. USA*, vol. 105, pp. 24–27, 2008.

[47] A. Ravasio *et al.*, "Single-shot diffractive imaging with a table-top femtosecond soft X-ray laser-harmonics source," *Phys. Rev. Lett.*, vol. 103, p. 028104, 2009.

[48] R. L. Sandberg *et al.*, "Tabletop soft-X-ray fourier transform holography with 50 nm resolution," *Opt. Lett.*, vol. 34, pp. 1618–1620, 2009.

[49] K. S. Raines *et al.*, "Three-dimensional structure determination from a single view," *Nature*, vol. 463, pp. 214–217, 2010.

[50] H. N. Chapman, "Femtosecond diffractive imaging with a soft-X-ray free-electron laser," *Nat. Phys.*, vol. 2, pp. 839–843, 2006.

[51] A. Barty *et al.*, "Ultrafast single-shot diffraction imaging of nanoscale dynamics," *Nat. Photon*, vol. 2, pp. 415–419, 2008.

[52] A. P. Mancuso *et al.*, "Coherent-pulse 2D crystallography using a free-electron laser X-ray source," *Phys. Rev. Lett.*, vol. 102, p. 035502, 2009.

[53] A. P. Mancuso *et al.*, "Coherent imaging of biological samples with femtosecond pulses at the free-electron laser FLASH," *New J. Phys.*, vol. 12, p. 035003, 2010.

[54] J. C. H. Spence *et al.*, "Phase recovery and lensless imaging by iterative methods in optical, X-ray and electron diffraction," *Philos.l Trans. Roy. Soc. London A, Math. Phys. Eng. Sci.*, vol. 360, pp. 875–895, 2002.

[55] J. Miao *et al.*, "Atomic resolution three-dimensional electron diffraction microscopy," *Phys. Rev. Lett.*, vol. 89, p. 155502, 2002.

[56] J. M. Zuo *et al.*, "Atomic resolution imaging of a carbon nanotube from diffraction intensities," *Science*, vol. 300, pp. 1419–1421, May 2003.

[57] O. Kamimura *et al.*, "Diffraction microscopy using 20 kV electron beam for multiwall carbon nanotubes," *Appl. Phys. Lett.*, vol. 92, p. 024106, 2008.

[58] S. Morishita *et al.*, "Diffractive imaging of the dumbbell structure in silicon by spherical-aberration-corrected electron diffraction," *Appl. Phys. Lett.*, vol. 93, p. 183103, 2008.

[59] R. Dronyak *et al.*, "Electron diffractive imaging of nano-objects using a guided method with a dynamic support," *Appl. Phys. Lett.*, vol. 95, p. 111908, 2009.

[60] J. Miao *et al.*, "Taking X-ray diffraction to the limit: Macromolecular structures from femtosecond X-ray pulses and diffraction microscopy of cells with synchrotron radiation," *Annu. Rev. Biophys. Biomol. Struct.*, vol. 33, pp. 157–176, 2004.

[61] I. Robinson and J. Miao, "Three-dimensional coherent X-ray diffraction microscopy," *MRS Bulletin*, vol. 29, pp. 177–181, 2004.

[62] J. Miao *et al.*, "Extending the methodology of X-ray crystallography to allow structure determination of non-crystalline materials, whole cells and single macromolecular complexes," *Annu. Rev. Phys. Chem.*, vol. 59, pp. 387–409, 2008.

[63] I. Robinson and R. Harder, "Coherent X-ray diffraction imaging of strain at the nanoscale," *Nat. Mater.*, vol. 8, pp. 291–298, 2009.

[64] K. Nugent, "Coherent methods in the X-ray sciences," *Adv. Phys.*, vol. 59, pp. 1–99, 2010.

[65] H. M. Quiney, "Coherent diffractive imaging using short wavelength light sources," *J. Mod. Opt.*, vol. 57, pp. 1109–1149, 2010.

[66] H. N. Chapman and K. A. Nugent, "Coherent lensless X-ray imaging," *Nat. Photon.*, vol. 4, pp. 833–839, 2010.

[67] A. P. Mancuso *et al.*, "Coherent diffractive imaging of biological samples at synchrotron and free electron laser facilities," *J. Biotechnol.*, vol. 149, pp. 229–237, 2010.

[68] S. Eisebitt *et al.*, "Lensless imaging of magnetic nanostructures by X-ray spectro-holography," *Nature*, vol. 432, pp. 885–888, 2004.

[69] S. Marchesini *et al.*, "Massively parallel X-ray holography," *Nat. Photon.*, vol. 2, pp. 560–563, 2008.

[70] D. Sayre, "Some implications of a theorem due to Shannon," *Acta Crystallogr.*, vol. 5, p. 843, 1952.

[71] R. W. Gerchberg and W. O. Saxton, "Practical algorithm for determination of phase from image and diffraction plane pictures," *Optik*, vol. 35, pp. 237–246, 1972.

[72] Y. M. Bruck and L. G. Sodin, "On the ambiguity of the image reconstruction problem," *Opt. Commun.*, vol. 30, pp. 304–308, 1979.

[73] M. H. Hayes, "The Reconstruction of a multidimensional sequence from the phase or magnitude of its fourier transform," *IEEE Trans. Accoust., Speech Signal Process.*, vol. ASP-30, no. 2, pp. 140–154, Apr. 1982.

[74] R. Bates, "Fourier phase problems are uniquely solvable in more than one dimension. I: Underlying theory," *Optik*, vol. 61, pp. 247–262, 1982.

[75] J. Miao and D. Sayre, "On possible extensions of X-ray crystallography through diffraction pattern oversampling," *Acta Crystallogr. A*, vol. 56, pp. 596–605, 2000.

[76] J. Miao *et al.*, "Phase retrieval of diffraction patterns from noncrystalline samples using the oversampling method," *Phys. Rev. B*, vol. 67, p. 174104, 2003.

[77] R. Xu *et al.*, "Coherent diffraction microscopy at SPring-8: Instrumentation, data acquisition and data analysis," *J. Synchrotron Radiat.*, vol. 18, pp. 293–298, 2011.

[78] Y. Takahashi *et al.*, "High-resolution diffraction microscopy using the plane-wave field of a nearly diffraction limited focused X-ray beam," *Phys. Rev. B, Condens. Matter*, vol. 80, p. 054103, 2009.

[79] Y. Takahashi *et al.*, "High-resolution projection image reconstruction of thick objects by hard X-ray diffraction microscopy," *Phys. Rev. B*, vol. 82, p. 214102, 2010.

[80] B. Abbey *et al.*, "Quantitative coherent diffractive imaging of an integrated circuit at a spatial resolution of 20 nm," *Appl. Phys. Lett.*, vol. 93, p. 214101, 2008.

[81] T. Pearsall, *Quantum Semiconductor Devices and Technologies*. Norwell, MA: Kluwer, 2000.

[82] J. Miao *et al.*, "Equally sloped tomography with oversampling reconstruction," *Phys. Rev. B*, vol. 72, p. 052103, 2005.

[83] E. Lee *et al.*, "Radiation dose reduction and image enhancement in biological imaging through equally-sloped tomography," *J. Struct. Biol.*, vol. 164, pp. 221–227, 2008.

[84] Y. Mao *et al.*, "Development and optimization of regularized tomographic reconstruction algorithms utilizing equally-sloped tomography," *IEEE Trans. Image Process.*, vol. 19, pp. 1259–1268, 2010.

[85] B. P. Fahimian *et al.*, "Low-dose X-ray phase-contrast and absorption CT using equally sloped tomography," *Phys. Med. Biol.*, vol. 55, pp. 5383–5400, 2010.

[86] J. Frank, *Electron Tomography: Three-Dimensional Imaging With the Transmission Electron Microscope*. vol. 167, New York: Plenum, 1992.

[87] V. Lucic *et al.*, "Structural studies by electron tomography: from cells to molecules," *Annu. Rev. Biochem.*, vol. 74, pp. 833–865, 2005.

[88] J. Kirz *et al.*, "Soft X-ray microscopes and their biological applications," *Quart. Rev. Biophys.*, vol. 28, pp. 33–130, 1995.

[89] M. A. Le Gros *et al.*, "X-ray tomography of whole cells," *Curr. Opin. Struct. Biol.*, vol. 15, pp. 593–600, 2005.

[90] R. Henderson, "The potential and limitations of neutrons, electrons and X-rays for atomic resolution microscopy of unstained biological molecules," *Quart. Rev. Biophys.*, vol. 28, pp. 171–93, 1995.

[91] Q. Shen *et al.*, "Diffractive imaging of nonperiodic materials with future coherent X-ray sources," *J. Synchrotron Radiat.*, vol. 11, pp. 432–438, 2004.

[92] M. R. Howells *et al.*, "An assessment of the resolution limitation due to radiation damage in X-ray diffraction microscopy," *J. Electron. Spectrosc. Rel. Phenom.*, vol. 170, pp. 4–12, 2009.

[93] H. C. Kapteyn *et al.*, "Extreme nonlinear optics: Coherent x rays from lasers," *Phys. Today*, vol. 58, pp. 39–46, 2005.

[94] D. Attwood, *Soft X-rays and Extreme Ultraviolet Radiation: Principles and Applications*. Cambridge, U.K.: Cambridge Univ. Press, 1999.

[95] S. Backus *et al.*, "High power ultrafast lasers," *Rev. Sci. Instrum.*, vol. 69, pp. 1207–1223, 1998.

[96] A. Rundquist *et al.*, "Phase-matched generation of coherent soft X-rays," *Science*, vol. 280, pp. 1412–1415, 1998.

[97] J. J. Rocca, "Table-top soft X-ray lasers," *Rev. Sci. Instrum.*, vol. 70, pp. 3799–3827, 1999.

[98] M. Berglund *et al.*, "Cryogenic liquid-jet target for debris-free laser-plasma soft X-ray generation," *Rev. Sci. Instrum.*, vol. 69, pp. 2361–2364, 1998.

[99] S. Kneip *et al.*, "Bright spatially coherent synchrotron X-rays from a table-top source," *Nat. Phys.*, vol. 6, pp. 980–983, 2010.

[100] A. Rousse *et al.*, "Production of a keV X-ray beam from synchrotron radiation in relativistic laser-plasma interaction," *Phys. Rev. Lett.*, vol. 93, p. 135005, 2004.

[101] M. Fuchs *et al.*, "Laser-driven soft-X-ray undulator source," *Nat. Phys.*, vol. 5, pp. 826–829, 2009.

[102] B. Dromey *et al.*, "Diffraction-limited performance and focusing of high harmonics from relativistic plasmas," *Nat. Phys.*, vol. 5, pp. 146–152, 2009.

[103] P. W. Wachulak *et al.*, "Sub 400 nm spatial resolution extreme ultraviolet holography with a table top laser," *Opt. Exp.*, vol. 14, pp. 9636–9642, 2006.

[104] P. W. Wachulak *et al.*, "Soft X-ray laser holography with wavelength resolution," *J. Opt. Soc. Amer. B*, vol. 25, pp. 1811–1814, 2008.

[105] R. A. Bartels *et al.*, "Generation of spatially coherent light at extreme ultraviolet wavelengths," *Science*, vol. 297, pp. 376–378, 2002.

[106] J. Schwenke *et al.*, "Single-shot holography using highorder harmonics," *J. Modern Opt.*, vol. 55, no. 16, pp. 2723–2730, 2008.

[107] M. C. Chou *et al.*, "Single-shot soft-X-ray digital holographic microscopy with an adjustable field of view and magnification," *Opt. Lett.*, vol. 34, pp. 623–625, 2009.

[108] D. Mai *et al.*, "Single-shot holography using high-order harmonics," *J. Mod. Opt.*, vol. 55, pp. 2723–2730, 2008.

[109] J. J. Rocca *et al.*, "Demonstration of a discharge pumped table-top soft-X-ray laser," *Phys. Rev. Lett.*, vol. 73, pp. 2192–2195, 1994.

[110] B. R. Benware *et al.*, "Demonstration of a high average power tabletop soft X-ray laser," *Phys. Rev. Lett.*, vol. 81, pp. 5804–5807, 1998.

[111] Y. Liu *et al.*, "Achievement of essentially full spatial coherence in a high-average-power soft-X-ray laser," *Phys. Rev. A*, vol. 63, p. 033802, 2001.

[112] Z. Chang *et al.*, "Generation of coherent soft X rays at 2.7 nm using high harmonics," *Phys. Rev. Lett.*, vol. 79, pp. 2967–2970, 1997.

[113] M. Nishikino *et al.*, "Demonstration of a soft-X-ray laser at 13.9 nm with full spatial coherence," *Phys. Rev. A*, vol. 68, p. 061802, 2003.

[114] P. Zeitoun *et al.*, "A high-intensity highly coherent soft X-ray femtosecond laser seeded by a high harmonic beam," *Nature*, vol. 431, pp. 426–429, 2004.

[115] P. B. Corkum, "Plasma perspective on strong field multiphoton ionization," *Phys. Rev. Lett.*, vol. 71, pp. 1994–1997, 1993.

[116] M. Lewenstein *et al.*, "Theory of high-harmonic generation by low-frequency laser fields," *Phys. Rev. A*, vol. 49, p. 2117, 1994.

[117] C. Spielmann *et al.*, "Generation of coherent X-rays in the water window using 5-femtosecond laser pulses," *Science*, vol. 278, pp. 661–664, Oct. 1997.

[118] J. Seres *et al.*, "Laser technology: Source of coherent kiloelectronvolt X-rays," *Nature*, vol. 433, pp. 596–596, 2005.

[119] A. Paul *et al.*, "Quasi-phase-matched generation of coherent extreme-ultraviolet light," *Nature*, vol. 421, pp. 51–54, 2003.

[120] A. Paul *et al.*, "Phase-matching techniques for coherent soft X-ray generation," *IEEE J. Quantum Electron.*, vol. 42, pp. 14–26, 2006.

[121] P. Balcou *et al.*, "Generalized phase-matching conditions for high harmonics: The role of field-gradient forces," *Phys. Rev. A*, vol. 55, pp. 3204–3210, 1997.

[122] A. Rundquist, "Phase-matched generation of coherent, ultrafast X-rays using high harmonics," Ph.D. dissertation, Dept. Phys., Washington State University, WA, 1998.

[123] C. G. Durfee III *et al.*, "Phase matching of high-order harmonics in hollow waveguides," *Phys. Rev. Lett.*, vol. 83, pp. 2187–2190, 1999.

[124] P. M. Paul *et al.*, "Observation of a train of attosecond pulses from high harmonic generation," *Science*, vol. 292, pp. 1689–1692, 2001.

[125] H. Kapteyn *et al.*, "Harnessing attosecond science in the quest for coherent X-rays," *Science*, vol. 317, pp. 775–778, 2007.

[126] A. L. Cavalieri *et al.*, "Attosecond spectroscopy in condensed matter," *Nature*, vol. 449, pp. 1029–1032, 2007.

[127] E. Goulielmakis *et al.*, "Single-cycle nonlinear optics," *Science*, vol. 320, pp. 1614–1617, 2008.

[128] Y. Wang *et al.*, "Phase-coherent, injection-seeded, table-top soft-X-ray lasers at 18.9 nm and 13.9 nm," *Nat. Photon*, vol. 2, pp. 94–98, 2008.

[129] J. J. Rocca *et al.*, "Soft-X-ray laser interferometry of a plasma with a tabletop laser and a Lloyd's mirror," *Opt. Lett.*, vol. 24, pp. 420–422, 1999.

[130] A.-S. Morlens *et al.*, "Submicrometer digital in-line holographic microscopy at 32 nm with high-order harmonics," *Opt. Lett.*, vol. 31, pp. 3095–3097, 2006.

[131] C. A. Brewer *et al.*, "Single-shot extreme ultraviolet laser imaging of nanostructures with wavelength resolution," *Opt. Lett.*, vol. 33, pp. 518–520, 2008.

[132] J. Spence, "Imaging technology: Harmonic pictures in a flash," *Nature*, vol. 449, pp. 553–554, 2007.

[133] M. M. Murnane and J. Miao, "Optics: Ultrafast X-ray photography," *Nature*, vol. 460, pp. 1088–1090, 2009.

[134] T. Popmintchev *et al.*, "Extended phase matching of high harmonics driven by mid-infrared light," *Opt. Lett.*, vol. 33, pp. 2128–2130, 2008.

[135] T. Popmintchev *et al.*, "Phase matching of high harmonic generation in the soft and hard X-ray regions of the spectrum," *Proc. Nat. Acad. Sci.*, vol. 106, pp. 10516–10521, 2009.

[136] M. C. Chen *et al.*, "Bright, coherent, ultrafast soft X-ray harmonics spanning the water window from a tabletop light source," *Phys. Rev. Lett.*, vol. 105, p. 173901, 2010.

[137] C. La-O-Vorakiat *et al.*, "Ultrafast demagnetization dynamics at the M edges of magnetic elements observed using a tabletop high-harmonic soft X-ray source," *Phys. Rev. Lett.*, vol. 103, p. 257402, 2009.

[138] M. E. Siemens *et al.*, "Quasi-ballistic thermal transport from nanoscale interfaces observed using ultrafast coherent soft X-ray beams," *Nat. Mater*, vol. 9, pp. 26–30, 2010.
[139] J. C. Solem and G. C. Baldwin, "Microholography of living organisms," *Science*, vol. 218, pp. 229–235, 1982.
[140] R. Neutze *et al.*, "Potential for biomolecular imaging with femtosecond X-ray pulses," *Nature*, vol. 406, pp. 752–757, 2000.
[141] J. Miao *et al.*, "An approach to three-dimensional structures of biomolecules by using single-molecule diffraction images," *Proc. Nat. Acad. Sci. USA*, vol. 98, pp. 6641–6645, 2001.
[142] R. Bonifacio *et al.*, "Collective instabilities and high-gain regime in a free electron laser," *Opt. Commun.*, vol. 50, pp. 373–378, 1984.
[143] P. Emma *et al.*, "First lasing and operation of an angstrom-wavelength free-electron laser," *Nat. Photon.*, vol. 4, pp. 641–647, 2010.
[144] T. Shintake *et al.*, "A compact free-electron laser for generating coherent radiation in the extreme ultraviolet region," *Nat. Photon*, vol. 2, pp. 555–559, 2008.
[145] V. Ayvazyan, "First operation of a free-electron laser generating GW power radiation at 32 nm wavelength," *Eur. Phys. J. D*, vol. 37, pp. 297–303, 2006.
[146] T. Shintake, "Possibility of single biomolecule imaging with coherent amplification of weak scattering X-ray photons," *Phys. Rev. E*, vol. 78, p. 041906, 2008.
[147] K. J. Gaffney and H. N. Chapman, "Imaging atomic structure and dynamics with ultrafast X-ray scattering," *Science*, vol. 316, pp. 1444–1448, 2007.
[148] M. J. Bogan *et al.*, "Single-shot femtosecond X-ray diffraction from randomly oriented ellipsoidal nanoparticles," *Phys. Rev. Spec. Top.—Accel. Beams*, vol. 13, p. 094701, 2010.
[149] M. J. Bogan *et al.*, "Single particle x-ray diffractive imaging," *Nano. Lett.*, vol. 8, pp. 310–316, 2007.
[150] N. D. Loh *et al.*, "Cryptotomography: Reconstructing 3D fourier intensities from randomly oriented single-shot diffraction patterns," *Phys. Rev. Lett.*, vol. 104, p. 225501, 2010.
[151] J. Frank, *Three-Dimensional Electron Microscopy of Macromolecular Assemblies*, 2nd ed. New York: Oxford Univ. Press, 2006.
[152] R. Fung *et al.*, "Structure from fleeting illumination of faint spinning objects in flight," *Nat. Phys.*, vol. 5, pp. 64–67, 2009.
[153] N.-T. D. Loh and V. Elser, "Reconstruction algorithm for single-particle diffraction imaging experiments," *Phys. Rev. E*, vol. 80, p. 026705, 2009.
[154] M. M. Seibert *et al.*, "Single mimivirus particles intercepted and imaged with an X-ray laser," *Nature*, vol. 470, pp. 78–81, 2011.
[155] (2011). [Online]. Available: www.physics.ucla.edu/research/imaging/Ankylography

Jianwei Miao received the B.S. degree from Hangzhou University, Zhejiang, China, in 1991, the M.S. degree from the Chinese Academy of Sciences, Beijing, China, in 1994, and the Ph.D. degree from the State University of New York, Stony Brook, in 1999, all in physics.

He joined the SLAC National Accelerator Laboratory in early 2000, and moved to the University of California, Los Angeles, in 2004. He is currently a Professor in the Department of Physics and Astronomy and the California NanoSystems Institute, University of California, Los Angeles. In 1998, he and collaborators proposed an explanation to the oversampling phasing method as well as the concept of the oversampling ratio. In 1999, he and colleagues performed the first demonstration experiment on CDI. Subsequently, in collaboration with Prof. T. Ishikawa at SPring-8/RIKEN, he and colleagues conducted the first 3-D CDI experiment in 2002, and first applied CDI to a biological specimen in 2003. In 2005, he and collaborators proposed EST for tomographic reconstruction from a limited number of projections. More recently, he and collaborators have proposed ankylography for 3-D structure determination from a single view.

Dr. Miao was the recipient of the Werner Meyer-Ilse Memorial Award in 1999 and the Alfred P. Sloan Research Fellowship in 2006. He is currently a Guest Professor of RIKEN, Hyogo, Japan, and of Zhejiang University, Zhejiang, China.

Richard L. Sandberg received the B.S. degree in physics from Brigham Young University, Provo, UT, in 2004 and the M.S. and Ph.D. degrees in physics and a certificate of optics in 2009 from the University of Colorado, Boulder, where he was an NSF IGERT Graduate Fellow in the Optical Science and Engineering Program.

He conducted a graduate internship with Advanced Micro Devices (AMD), Inc., in the Fall of 2006. He was a Director's Postdoctoral Fellow in the Center for Advanced Solar Photophysics and the Physical Chemistry and Advanced Spectroscopy Group, Chemistry Division at Los Alamos National Laboratory, Los Alamos, NM. In 2007, he and collaborators were the first to perform coherent diffractive imaging on a coherent tabletop soft X-ray sources.

Dr. Sandberg was the recipient of the 2008 Optical Society of America's New Focus/Bookham Student Award.

Changyong Song received the B.S. degree in physics from Jeonbuk National University, Jeonju, Korea, in 1995 and the Ph.D. degree in experimental condensed matter physics from Iowa State University, Ames, in 2001.

He was a Postdoctoral Researcher at Pohang University of Science and Technology (POSTECH), Pohang, Korea, from 2001 to 2004 and at University of California, Los Angeles, from 2004 to 2008. In March 2008, he joined RIKEN, Hyogo, Japan, where he has been developing an innovative X-ray diffraction microscope by using the Japanese X-Ray Free Electron Laser at SPring-8.

Dr. Song is currently an Initiative Research Scientist at the Song Initiative Research Unit of RIKEN and an Adjunct Professor of physics at POSTECH.